Upregulation of virulence genes promotes *Vibrio cholerae* biofilm hyperinfectivity

A. L. Gallego-Hernandez[a,1], W. H. DePas[b,1], J. H. Park[a,1], J. K. Teschler[a,1], R. Hartmann[c,d], H. Jeckel[c,d], K. Drescher[c,d], S. Beyhan[e], D. K. Newman[b,2], and F. H. Yildiz[a,2]

[a]Department of Microbiology and Environmental Toxicology, University of California, Santa Cruz, CA 95064; [b]Division of Biology and Biological Engineering, California Institute of Technology, Pasadena, CA 91125.; [c]Max Planck Institute for Terrestrial Microbiology, D-35043 Marburg, Germany; [d]Department of Physics, Philipps University Marburg, D-35032 Marburg, Germany; and [e]Department of Infectious Diseases, J. Craig Venter Institute, La Jolla, CA 92037

Edited by John J. Mekalanos, Harvard University, Boston, MA, and approved March 11, 2020 (received for review September 23, 2019)

Vibrio cholerae **remains a major global health threat, disproportionately impacting parts of the world without adequate infrastructure and sanitation resources. In aquatic environments, *V. cholerae* exists both as planktonic cells and as biofilms, which are held together by an extracellular matrix. *V. cholerae* biofilms have been shown to be hyperinfective, but the mechanism of hyperinfectivity is unclear. Here we show that biofilm-grown cells, irrespective of the surfaces on which they are formed, are able to markedly outcompete planktonic-grown cells in the infant mouse. Using an imaging technique designed to render intestinal tissue optically transparent and preserve the spatial integrity of infected intestines, we reveal and compare three-dimensional *V. cholerae* colonization patterns of planktonic-grown and biofilm-grown cells. Quantitative image analyses show that *V. cholerae* colonizes mainly the medial portion of the small intestine and that both the abundance and localization patterns of biofilm-grown cells differ from that of planktonic-grown cells. In vitro biofilm-grown cells activate expression of the virulence cascade, including the toxin coregulated pilus (TCP), and are able to acquire the cholera toxin-carrying CTXΦ phage. Overall, virulence factor gene expression is also higher in vivo when infected with biofilm-grown cells, and modulation of their regulation is sufficient to cause the biofilm hyperinfectivity phenotype. Together, these results indicate that the altered biogeography of biofilm-grown cells and their enhanced production of virulence factors in the intestine underpin the biofilm hyperinfectivity phenotype.**

Vibrio cholerae | hyperinfectivity | biofilm | gastrointestinal infection

Cholera is an acute diarrheal illness caused by the ingestion of the pathogenic bacterium *Vibrio cholerae* in contaminated drinking water and food. It remains a major public health concern in the 21st century, and improvements in mitigation measures are needed to alleviate its impact (1, 2). *V. cholerae* occurs naturally in various aquatic environments. Its ability to survive in these habitats is tied to its capacity to cause cholera outbreaks when it is transmitted to a human host.

One key factor that is predicted to be important for the infection cycle of *V. cholerae* is its ability to form biofilms, which are matrix-enclosed, surface-associated cellular communities (3–5). Biofilm formation increases environmental fitness of *V. cholerae* in natural settings by providing protection from a number of environmental stresses, including predation by protozoa and bacteriophages (6, 7). In cholera endemic areas, removal of particles >20 μm in diameter from surface waters can reduce cholera incidence by 48%, suggesting that biofilms are critical for the transmission of *V. cholerae* (8). Stool samples from cholera patients contain *V. cholerae* both as planktonic cells and biofilm aggregates; the average infectivity of the biofilm aggregates is significantly higher than that of planktonic cells (9–11). Maintenance of biofilm architectural properties appears to be dispensable for this phenotype, as both intact and dispersed biofilms are markedly more infectious than free-living cells (3).

Taken together, these studies underscore the significance of the biofilm growth mode in the environmental, transmission, and infectivity phases of *V. cholerae*'s life cycle. Despite this awareness, the molecular mechanisms responsible for the biofilm-related hyperinfectious phenotype in *V. cholerae* are poorly understood. Here we demonstrate that the altered biogeography of biofilm-grown cells and enhanced production of virulence factors by biofilm-grown cells govern the biofilm hyperinfectivity phenotype.

Results and Discussion

V. cholerae **Biofilms Are Hyperinfectious.** To further understand the hyperinfectivity mechanisms of biofilm-grown *V. cholerae* cells, we grew *V. cholerae* biofilms on different surfaces (plastic, glass, and chitin) and compared the ability of planktonic-grown and biofilm-grown cells to colonize the infant mouse intestine using a competitive index (CI) assay. In each case, biofilm-grown cells colonized the small intestine ∼7–10 times more effectively than planktonic-grown cells (Fig. 1*A*). Mice infected with biofilm-grown cells also exhibited more severe diarrheal symptoms, as

Significance

Vibrio cholerae **biofilms are hyperinfectious, yet the mechanisms underpinning this phenomenon remain poorly understood. We analyzed *V. cholerae* intestinal infection in three-dimensional space, using imaging and quantification tools and uncovered differences in the biogeography of the small intestine infected with biofilm-grown cells compared to planktonic-grown cells. Our experiments show that *V. cholerae* biofilm-grown cells upregulate virulence factors compared to planktonic-grown cells, priming biofilm-grown cells for infection and driving a hyperinfectious biofilm phenotype. Collectively, this work establishes a method for studying *V. cholerae* infection and enhances our understanding of *V. cholerae* virulence mechanisms and the importance of biofilms in contributing to acute infections.**

Author contributions: A.L.G.-H., W.H.D., J.H.P., J.K.T., K.D., D.K.N., and F.H.Y. designed research; A.L.G.-H., W.H.D., J.H.P., and J.K.T. performed research; R.H. contributed new reagents/analytic tools; A.L.G.-H., W.H.D., J.H.P., J.K.T., R.H., H.J., K.D., S.B., D.K.N., and F.H.Y. analyzed data; and A.L.G.-H., W.H.D., J.H.P., J.K.T., K.D., D.K.N., and F.H.Y. wrote the paper.

The authors declare no competing interest.

This article is a PNAS Direct Submission.

Data deposition: RNA-seq data are available through National Center for Biotechnology Information (NCBI) Gene Expression Omnibus (GEO) (series number GSE135887).

[1]A.L.G.-H., W.H.D., J.H.P., and J.K.T. contributed equally to this work.

[2]To whom correspondence may be addressed. Email: dkn@caltech.edu or fyildiz@ucsc.edu.

This article contains supporting information online at https://www.pnas.org/lookup/suppl/doi:10.1073/pnas.1916571117/-/DCSupplemental.

First published April 30, 2020.

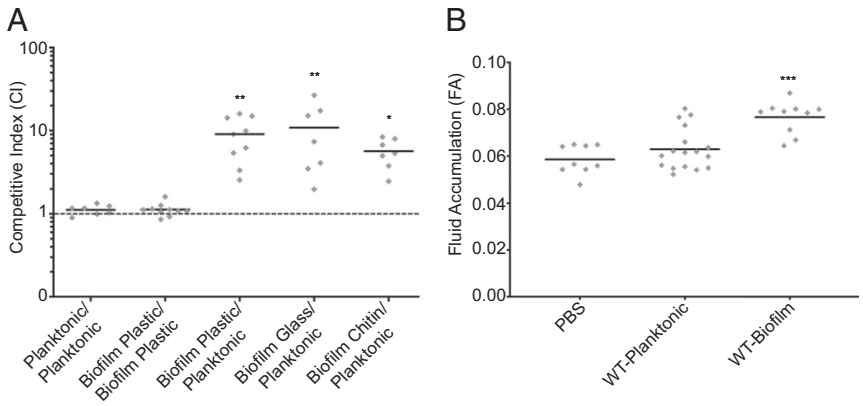

Fig. 1. Biofilm-grown cells are more virulent than planktonic-grown cells. (*A*) The ability of *V. cholerae* planktonic and biofilm-grown cells to colonize the infant mouse intestine was analyzed using a competition assay, resulting in the measurement of a CI that compares the wild-type *V. cholerae* grown in different conditions prior to intragastrical inoculation: Planktonic indicates that cells were grown planktonically, Biofilm Plastic indicates that biofilms were grown in plastic tubes, Biofilm Glass indicates that biofilms were grown on glass slides, and Biofilm Chitin indicates that biofilms were grown on chitin. Each symbol represents the CI in an individual mouse ($n \geq 7$); horizontal bars indicate the mean. Statistical analysis was carried out using a one-way ANOVA and Kruskal-Wallis test (*$P < 0.05$, **$P < 0.005$). (*B*) Fluid accumulation (FA) ratio was measured in mice infected with a PBS control, wild-type planktonic-grown, or wild-type plastic tube–biofilm-grown cells ($n \geq 9$). Statistical analysis was carried out using a one-way ANOVA and Kruskal-Wallis test (***$P < 0.0001$).

measured by fluid accumulation (Fig. 1*B*). These findings demonstrate that biofilm-grown cells, regardless of the surface on which they are formed, are in a hyperinfectious state and are able to better colonize the infant mouse intestine than planktonic-grown cells.

Abundance and Spatial Patterns of Colonization Are Altered in Intestines Infected with Biofilm-Grown Cells. The geography of a colonization site directly affects microbial activity, including processes that determine virulence (12). We hypothesized that planktonic-grown and biofilm-grown cells may have altered colonization niches that contribute to the hyperinfectivity of biofilm-grown cells. To test this, we paired quantitative three-dimensional (3D) confocal microscopy with microbial identification after passive CLARITY technique (MiPACT) to analyze *V. cholerae* infection outcomes of planktonic-grown and biofilm-grown bacteria in the intestine, using a murine model of infection (13). MiPACT involves fixing and embedding tissue in an acrylamide hydrogel to provide structural integrity (important for the often mucous-rich and unstable sites of bacterial colonization) and subsequent optical clearing of the tissue to allow deep imaging (14, 15). Hybridization chain reaction (HCR) was then used to label bacterial ribosomal RNA (rRNA) and messenger RNA (mRNA) to identify cells and quantify their activity in the context of their spatial arrangement (16–18). The *tcpA* mRNA probe was validated in vitro in pTAC::*toxT*, pTAC::*toxT*Δ*tcpA*, wild-type (WT), and Δ*tcpA* strains and in vivo in phosphate-buffered saline (PBS)-infected intestines (*SI Appendix*, Fig. S4 *A–C*). The *V. cholerae* specific rRNA probe was also validated in vivo in PBS-infected intestines (*SI Appendix*, Fig. S4*D*). By applying this technique to infected intestines, we were able to comprehensively characterize *V. cholerae* colonization in the 3D intestinal space (Fig. 2 *A* and *B*).

To quantify bacterial biomass and evaluate the spatial distribution pattern in the intestine, images were analyzed using BiofilmQ, a software tool we developed for quantifying spatially resolved biofilm properties (19). For both biofilm- and planktonic-grown cell infections, we observed that the majority of the cells were found in the medial portion of the intestine (sections 2 and 3), consistent with previous observations (Fig. 2 *D* and *E* and *SI Appendix*, Figs. S1 and S2) (20). We therefore focused on these regions for the remainder of our analysis (Fig. 2 *C–E* and Movies S1 and S2). In the medial segment of the intestine, total biomass of biofilm-grown cells was consistently observed to be much more abundant than planktonic-grown cells (4-fold), indicating that biofilm-grown cells were more efficient at colonizing within that niche (Fig. 2*D*). While the bacterial load was lower in the proximal and distal portions of the small intestine, biofilm-grown cells were still more successful at colonizing these regions (*SI Appendix*, Figs. S1 and S2). Quantitative analysis of the fraction of intestinal surface that has been colonized also showed that biofilm-grown cells colonized a greater portion of the intestine than planktonic-grown cells (Fig. 2*E*). It is important to note that due to increased fluid accumulation in mice infected with biofilm-grown cells, their abundance could be underestimated at late infection (Fig. 1*B*).

With respect to the spatial distribution, we observed that planktonic-grown cells were predominantly found along the bottom half of the villi, consistent with previous reports (20). In contrast, a greater proportion of biofilm-grown cells were localized to the top half of the villi (Fig. 2*F*). Preferential localization of planktonic-grown cells to the base of the villi has been suggested to protect cells from peristalsis in the lumen (20). Localization of biofilms to the top half of the villi may indicate that these cells can adhere more tightly and, furthermore, that this location may protect cells from host-associated defenses produced in the crypts (21). This spatial preference may contribute to the increased bacterial load observed in mice infected with biofilm-grown cells. Application of detection and quantification techniques allowed us to reveal that planktonic-grown and biofilm-grown cells exhibit differences in colonization and spatial distribution along the intestine.

Enhanced Production of Virulence Factors Accounts for Biofilm Hyperinfectivity Phenotype. We next sought to identify the mechanism by which biofilms become hyperinfectious. To do this we first compared whole-genome expression profiles of cells from biofilms grown on plastic surfaces and planktonic-grown cells (22). As expected, transcript abundance of genes involved in the biofilm matrix assembly, including the key biofilm regulators *vpsR* and *vpsT* and *Vibrio* polysaccharide (*vps*) genes, was higher in cells grown in biofilms, and transcript abundance of genes involved in flagellar motility was decreased in cells grown in biofilms (Fig. 3 *A* and *B*). In addition to these expected differences, message abundance of a number of virulence-related

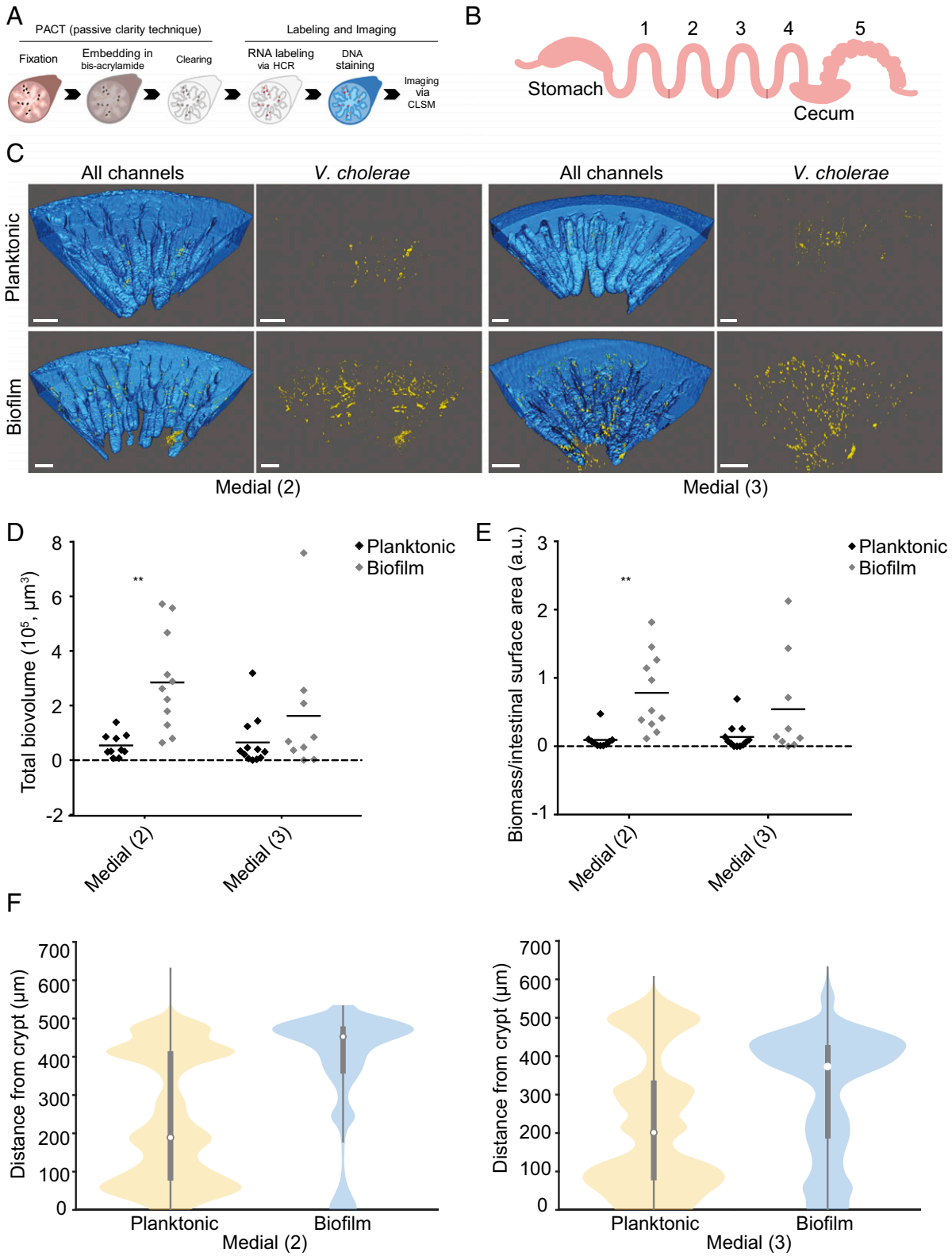

Fig. 2. MiPACT imaging of infected infant mouse intestines reveals differences in abundance and spatial patterns of colonization between planktonic-grown and biofilm-grown cells. (*A*) Schematic showing the MiPACT and HCR protocol. CLSM, confocal laser scanning microscopy. (*B*) Mouse gastrointestinal tract sections: proximal (section 1), medial (sections 2 and 3), and distal (section 4). The large intestine was treated as one section (section 5). From the central regions of these sections, 1-mm segments were used for tissue clearing, HCR treatment, staining, and imaging. (*C*) Three-dimensional rendering of the medial sections of the small intestine infected with planktonic- or biofilm-grown *V. cholerae* (showing representative images from $n \geq 9$ taken from 4 to 5 mice). (Scale bar, 100 μm.) (*D*) Total biovolume of cells found in sections 2 and 3 of the intestines infected with planktonic- or biofilm-grown cells ($n \geq 9$). Statistical analysis was carried out using an unpaired two-sample *t* test (**$P < 0.005$). (*E*) Bacterial biomass volume normalized by the intestinal surface area in medial sections of the intestines ($n \geq 9$). Statistical analysis was carried out using an unpaired two-sample *t* test (**$P < 0.005$). (*F*) Spatial distribution of planktonic and biofilm-grown cells along the villi of the intestines in sections 2 and 3 of the intestines ($n \geq 9$).

genes was increased in biofilm-grown cells, including the major virulence regulators *toxT*, *toxR*, *toxS*, *tcpP*, and *tcpH* as well as the crucial virulence factors regulated by them. These include the toxin-coregulated pilus (TCP), a Type IV pilus that is required for intestinal colonization, and cholera toxin (CTX), a secreted enterotoxin responsible for inducing the watery diarrhea associated with cholera (Fig. 3 *A* and *B*) (23–25). We confirmed that expression of *vpsL*, *tcpA*, and *ctxA* was indeed higher in biofilm-grown cells using qPCR as a complementary approach (*SI Appendix*, Fig. S3*A*).

TCP is also a receptor for the CTXΦ, which is a lysogenic bacteriophage carrying the CTX gene cluster that can infect nonpathogenic *Vibrio* species and confer virulence to these strains (26). Given that TCP transcript levels were more

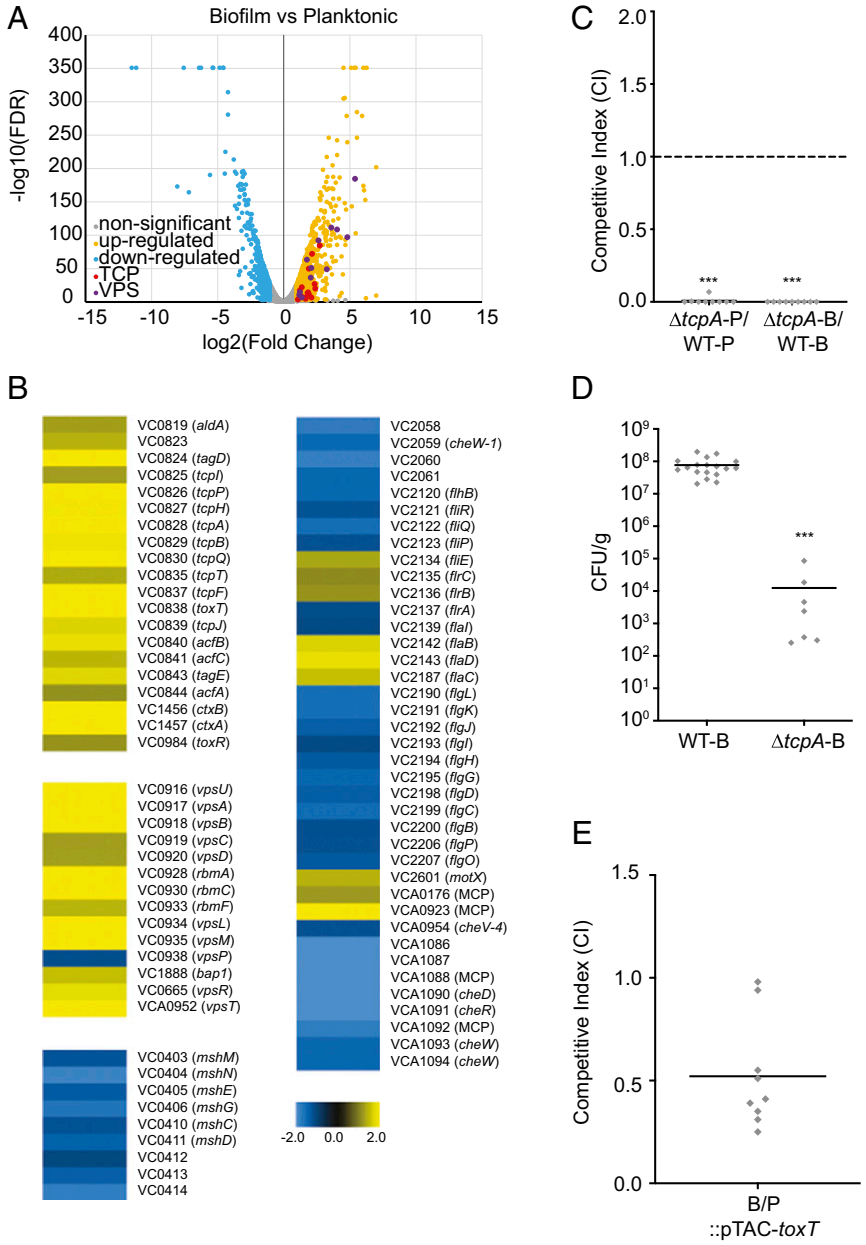

Fig. 3. Up-regulation of virulence genes in biofilm-grown cells contributes to the hyperinfectious phenotype. (*A*) RNA-seq analysis was performed comparing gene expression in plastic tube-biofilm and planktonic-grown cells. Volcano plot of differentially expressed genes (fold change [FC] of >2, $P < 0.05$) between cells grown in biofilms or planktonically ($n = 3$). The negative log of false discovery rate (FDR) (base 10) is plotted on the *y* axis, and the log of the FC (base 2) is plotted on the *x* axis. (*B*) Heat maps of differentially expressed genes that are up-regulated or down-regulated in both cell states. The color bar indicates fold change up or down in biofilm-grown cells, with blue indicating that genes are significantly down-regulated in biofilms and yellow indicating that genes are significantly up-regulated in biofilms ($n = 3$). (*C*) Ability of Δ*tcpA* strains to colonize the infant mouse intestine in either a planktonic- or biofilm-grown state were analyzed using a competition assay with an isogenic wild-type strain. P stands for planktonic, and B stands for plastic tube–biofilm-grown cells. Each symbol represents the CI in an individual mouse ($n = 9$); horizontal bars indicate the mean. Statistical analysis was carried out using a one-way ANOVA and Dunnett's multiple-comparison test (***$P < 0.001$). (*D*) Single-strain infections were carried out to determine cfu per gram of small intestine for biofilm-grown wild-type and Δ*tcpA* strains ($n = 9$). Statistical analysis was carried out using an unpaired two-sample *t* test (***$P < 0.001$). (*E*) *tcp* and virulence gene expression was controlled by placing *toxT* under the control of an IPTG-inducible promoter. Virulence gene expression was then modulated to equivalent levels in *V. cholerae* planktonic- and biofilm-grown cells. P stands for planktonic, and B stands for plastic tube–biofilm-grown cells. These cells were then tested for their ability to colonize the infant mouse intestine using a competition assay with an isogenic wild-type strain ($n = 9$).

abundant in biofilm-grown cells than planktonic-grown cells, we reasoned that biofilm-grown cells would undergo increased transduction events compared to planktonic-grown cells (26). CTXΦ also encode for repressors of CTXΦ replication, thus preventing a secondary infection by an identical phage (27, 28). Therefore, to test our hypothesis, we first generated a strain lacking one of the CTXΦ repressors (ΔVC1464) to overcome phage immunity. We then assessed the transduction efficiency of cells transduced in either biofilm-grown or planktonic-grown cells and observed that biofilm-grown cells were transduced ~1,000-fold more than planktonic-grown cells (Table 1). This finding not only confirms that TCP is more abundant in biofilms but also indicates that the biofilm growth mode likely contributes to the evolution of pathogenic strains of *V. cholerae* and hyperinfectivity once *ctx* genes are acquired.

Overall transcript abundance of virulence genes was higher under biofilm conditions indicating that biofilm-grown cells might be primed for host infection. To test this, we first assayed the ability of planktonic-grown and biofilm-grown Δ*tcpA* cells to compete with wild type during intestinal colonization. Under both conditions, the Δ*tcpA* strain was unable to colonize as well as wild type, exhibiting more than a 125-fold decrease in colonization (Fig. 3*C*). Additionally, single-strain colonization assays with biofilm-grown wild type or biofilm-grown Δ*tcpA* cells showed an even greater defect in intestinal colonization, as the *tcpA* mutant abundance in the intestine was decreased 6,000-fold compared to wild type (Fig. 3*D*). However, additional virulence factors could also contribute to the biofilm hyperinfectivity phenotype in addition to TCP. Because transcriptomic analyses showed that *toxT*, the most downstream regulator of the virulence cascade, is more abundant in biofilm-grown than planktonic cells, we decided to selectively control its expression as a different way of probing the hyperinfectivity phenotype. We modulated expression of *toxT* from an isopropyl β-D-1-thiogalactopyranoside (IPTG) inducible promoter (P*tac* promoter) to similar levels in both planktonic and biofilm-grown cells and performed a competition assay (*SI Appendix*, Fig. S3 *B* and *C*). Under these conditions, biofilm-grown cells no longer outcompeted planktonic-grown cells, and planktonic-grown cells demonstrated a slight advantage in intestinal colonization (Fig. 3*E*). This finding supports the hypothesis that biofilm-induced up-regulation of virulence genes is the key contributor to the hyperinfectivity phenotype of *V. cholerae* biofilm cells.

Based on these results, we predicted that biofilm-grown cells would express TCP more highly in the intestine than planktonic-grown cells. To test this prediction in situ, we used MiPACT and HCR. We were able to detect and localize the *tcp* message in 3D space within infected intestinal samples (Fig. 4*A*). Using BiofilmQ, we quantified *tcpA* mRNA using two different metrics. Analysis of *tcpA* signal, normalized by biomass (Fig. 4*B*), demonstrated that 22 h postinoculation, at late-stage infection, *tcpA* is similarly expressed in planktonic and biofilm-grown cells. However, given the overall increased bacterial load per intestinal surface area for biofilm-infected intestines (Fig. 2*E*), the overall *tcpA* abundance per intestinal surface area was also higher (Fig. 4*C*). Collectively, these results showed that biofilm-grown cells highly express *tcpA* prior to infection and that biofilm-infected intestines have enhanced levels of *tcpA* mRNA, thereby contributing to the enhanced adherence, colonization, and severity of the disease.

Table 1. CTX-Kmϕ transduction of planktonic-grown or biofilm-grown cells

Strain	Growth Mode	CTX-Kmϕ Transduction Efficiency
ΔVC1464	Planktonic-grown cells	3 cfu/mL
ΔVC1464	Biofilm-grown cells	3×10^{3}*** cfu/mL

Statistical analysis was carried out using an unpaired two-sample *t* test (***$P < 0.0001$).

The contribution of biofilms in chronic infections to antimicrobial resistance and protection from host defenses is well established; however, the role of biofilms in acute infections is less understood (29). In *Pseudomonas aeruginosa* and *Staphylococcus aureus*, it is generally accepted that acute infection is marked by rapidly replicating bacteria producing high levels of virulence factors, while chronic infection is marked by slower-growing bacteria adhering to tissues or another surface to form biofilms (30). However, the growth state of bacteria during infection is often dynamic, and very little work has been done to compare the impact of planktonic-grown cells and biofilm-grown cells on transmission and initiation of acute infection. In *V. cholerae*, biofilm-grown cells require a lower infectious dose (lower ID_{50}), grow faster during acute infection, achieve a higher level of colonization, and exhibit different temporal infection dynamics in the small intestines of infant mice, compared with the cells that were grown planktonically (3, 31).

We discovered that biofilm-grown *V. cholerae* cells are primed for enhanced infectivity by producing the core virulence factors TCP and CTX. Previous work demonstrated that the master biofilm regulator, VpsR, positively regulates AphA, a positive upstream regulator of virulence factors (32–34). This regulatory pathway could contribute to the enhanced expression of virulence factors during biofilm formation. The quorum-sensing regulator, HapR, has been shown to impact hyperinfectivity in intact biofilms, but is dispensable in dispersed biofilms (3, 35). This suggests that HapR likely mediates detachment from the biofilm in vivo and that detachment during infection may be required to fully unlock the biofilm hyperinfectivity phenotype. It is known that HapR negatively regulates AphA, indicating that virulence production during different stages of infection is tightly controlled by numerous regulators (36). We additionally showed that, due to the enhanced TCP production, biofilms are likely to be hotbeds for phage transduction and the generation of toxigenic *V. cholerae* variants. More broadly, our imaging and quantification methods provide biological insights into *Vibrio* biofilm-mediated hyperinfectivity and technical advancements that will enhance our understanding of other biofilm-related pathogens in the context of the host.

Materials and Methods

Ethics Statement. All animal procedures used were in strict accordance with the *Guide for the Care and Use of Laboratory Animals* (37) and were approved by the University of California (UC), Santa Cruz, Institutional Animal Care and Use Committee, Santa Cruz, CA (approval number Yildf1206).

Bacterial Strains, Plasmids, and Culture Conditions. The strains used in this study are listed in the *SI Appendix*, Table S1. *V. cholerae* and *Escherichia coli* strains were grown aerobically in Lysogeny-Broth (LB) broth (1% tryptone, 0.5% yeast extract, 1% NaCl [pH 7.5]) at 30 °C and 37 °C, respectively. LB agar contained granulated agar (Difco, Becton Dickinson) at 1.5% (wt/vol). Planktonic cultures were grown in 5 mL LB at 30 °C for 16 h under shaking conditions (200 rpm). Biofilms were grown as follows: for biofilms grown in plastic tubes, cells were grown in 15-cm silicon tubes (ID 0.125/OD 0.250) with 2% LB medium (0.02% tryptone, 0.01% yeast extract, 1% NaCl [pH 7.5]) and incubated at room temperature for 48 h using a peristaltic pump to deliver constant flow at a rate of 4.4 mL per hour; biofilms on chitin and glass surfaces were formed using drip flow reactors in LB medium. Biofilm-grown cells were prepared by scraping into 1× PBS and resuspended by pipetting. Medium additives were used when necessary at the following concentrations: rifampin, 100 μg/mL; ampicillin, 100 μg/mL; kanamycin, 50 μg/mL; and IPTG, 1 mM.

DNA Manipulations. Plasmids were constructed using the Gibson assembly recombinant DNA technique (New England BioLabs). Gene deletions were carried out using allelic exchange of the native open reading frame (ORF) with the truncated ORF, as previously described (38). The deletion constructs

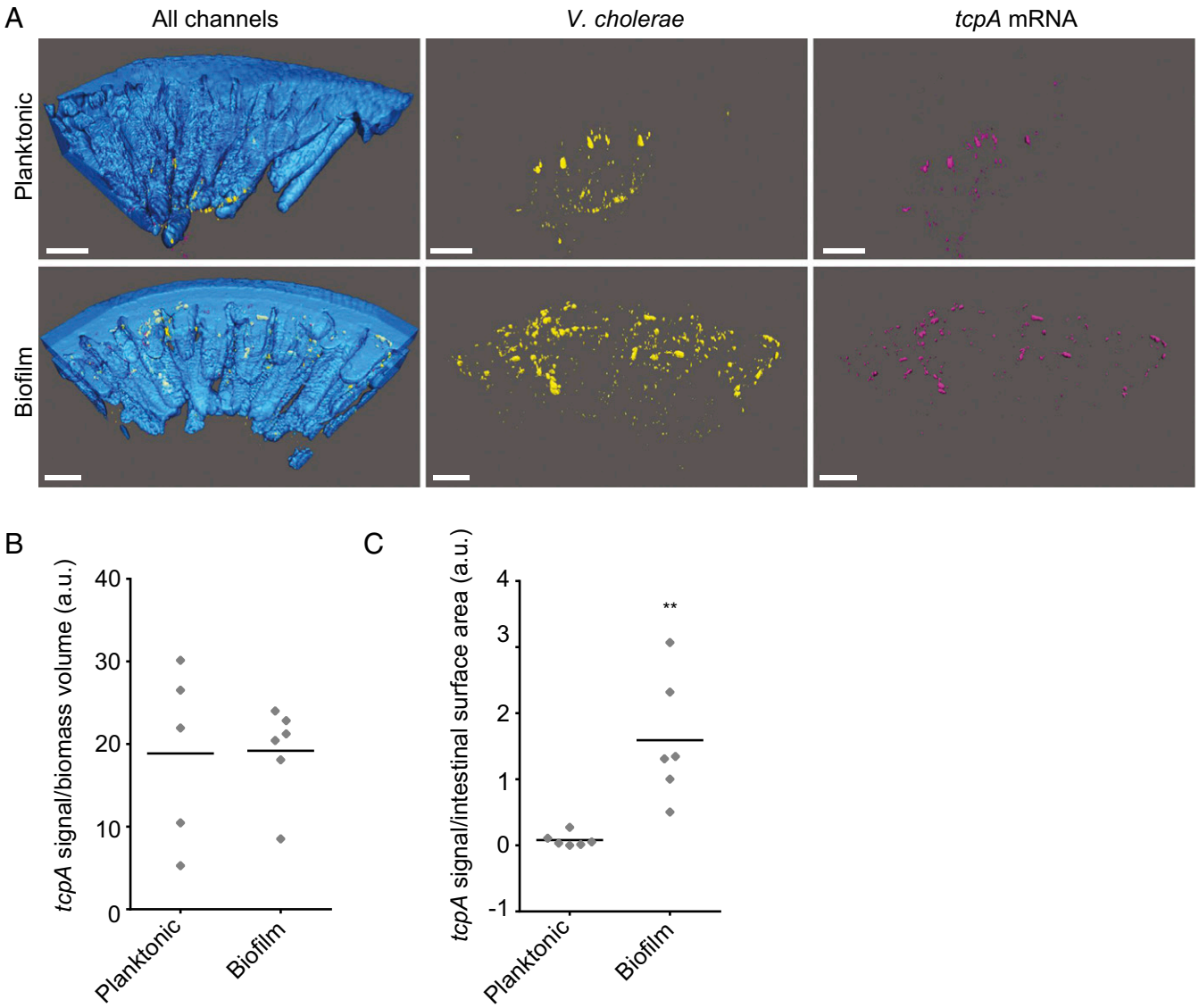

Fig. 4. Biofilm-grown cells enhance total *tcp* expression in vivo. (*A*) Three-dimensional rendering of the medial section of the small intestine infected with planktonic- or biofilm-grown *V. cholerae* expressing *tcpA* ($n = 6$). (Scale bar, 100 μm.) (*B*) Abundance of *tcpA* transcript HCR fluorescence signal per bacterial biomass volume of cells found in medial sections of the intestines infected with planktonic- or biofilm-grown cells ($n \geq 5$). Statistical analysis was carried out using an unpaired two-sample *t* test. (*C*) Abundance of *tcpA* transcript signal per intestinal surface area (including villi and crypts) found in medial sections of the intestines infected with planktonic- or biofilm-grown cells ($n \geq 5$). Statistical analysis was carried out using an unpaired two-sample *t* test (**$P < 0.005$).

were sequenced (UC Berkeley DNA Sequencing Facility) and are listed in the *SI Appendix*, Table S1.

Competitive Index. An in vivo competition assay for intestinal colonization determination was performed as described previously (39). Five-day-old suckling CD-1 mice were inoculated intragastrically with 10^6 cells that were in planktonic- or biofilm-growth mode as indicated. This inoculum consisted of a mixture of two strains, at ∼1:1 colony-forming units (cfu) ratio, suspended in PBS. The two strains in this mixture were the *V. cholerae* Δ*lacZ* control strain and *V. cholerae* wild-type or mutant strains. The inoculum was plated on LB agar plates containing 5-bromo-4-chloro-3-indoyl-β-D-galactopyranoside (X-Gal) to differentiate the colonies of the Δ*lacZ* strain and the other strains and to determine the input ratio. At 22 h postinoculation, small intestines were removed, weighed, homogenized, and plated on appropriate selective and differential media to enumerate strain (wild-type or mutant)/condition #1 (planktonic-grown or biofilm-grown) and strain (wild-type or mutant)/condition #2 (planktonic-grown or biofilm-grown) cells recovered to obtain the output ratios. In vivo competitive indices were calculated by dividing the small-intestine output ratio of strain (wild-type or mutant)/condition #1 (planktonic-grown or biofilm-grown) to strain (wild-type or mutant)/condition #2 (planktonic-grown or biofilm-grown) by the inoculum input ratio of strain/condition #1 to strain (wild-type or mutant)/condition #2 (planktonic-grown or biofilm-grown).

Fluid Accumulation. After *V. cholerae* oral inoculation as indicated previously, mice were sacrificed 22 h postinfection, and the fluid accumulation (FA) ratio was determined as: weight of stomach and intestines (gut)/(mouse body weight − gut weight) (40). All animal procedures used were in strict accordance with the NIH *Guide for the Care and Use of Laboratory Animals* (37) and were approved by the UC Santa Cruz Institutional Animal Care and Use Committee (Yildf1806).

RNA Isolation. *V. cholerae* wild-type cells were grown in planktonic or biofilm mode as described above. Cells were collected and supernatant removed after centrifugation. Pellets were immediately resuspended in 2 mL of TRIzol (Invitrogen) and stored at −80 °C. Total RNA was isolated according to the TRIzol manufacturer's instructions. To remove contaminating DNA, total RNA was incubated with RNase-free DNase I (Ambion), and RNeasy mini kit

(Qiagen), and ethanol precipitation was used to clean up RNA after DNase digestion. The RNA concentration was determined with a NanoDrop spectrophotometer (ThermoFisher), and the RNA quality was evaluated using a 2100 Bioanalyzer (Agilent Technologies). Three biological replicates were generated for each condition.

Complementary DNA (cDNA) Library Construction and Illumina HiSeq Sequencing. Total RNA (5 μg) was treated with a MICROBExpress Kit (Ambion) to remove ribosomal RNA, and the efficiency was confirmed using a 2100 Bioanalyzer. Libraries for RNA-seq were prepared using NEBNext Ultra Directional RNA Library Prep Kit for Illumina (New England Biolabs). Twelve indexed samples were sequenced per single lane using the HiSeq4000 Illumina sequencing platform for 100-bp single reads (UC Davis Genome Center, UC Davis, CA).

RNA-Seq Informatics Analysis. Raw reads were quality-trimmed and mapped to the *V. cholerae* genome using J. Craig Venter Institute's in-house pipeline. Briefly, rRNA reads were filtered using riboPicker version 2.4.3 (41), and nonrRNA reads were mapped to *V. cholerae* O1 biovar El Tor str. N16961 (assembly GCA_000006745.1) transcripts using CLC-NGS Cell version 4.4.2 (Qiagen). Significantly regulated genes were determined using EdgeR (42); a fold change greater than 2.0 and a false discovery rate of less than 1% were used as a cutoff.

Quantitative Real Time PCR. RNA was isolated as described above. The reverse transcription reaction to generate cDNA was carried out using the SuperScript III Reverse Transcriptase (Invitrogen) according to the manufacturer's instructions; briefly, 1 μg of RNA in a 20-μL final volume was incubated at 25 °C for 5 min, 50 °C for 1h, and 70 °C for 15 min. The product was used in a PCR using suitable primers, and RNA without reverse transcriptase treatment was used as a negative control. For qRT-PCR expression analysis, real-time PCR was performed using a Bio-Rad CFX1000 thermal cycler and Bio-Rad CFX96 real-time imager with specific primer pairs (designed within the coding region of the target gene) and SsoAdvanced SYBR green supermix (Bio-Rad). Results are from $n = 3$–4 independent experiments, each performed in triplicate. All samples were normalized to the expression of the housekeeping gene *recA* using the ΔΔCt method.

Transduction Assays. CTX-kanamycin (Km) Φ was isolated by growing *V. cholerae* O395 (pCTX-Km) overnight in 5 mL LB with kanamycin (50 μg/mL), pH 8.5 at 37 °C and filtering supernatant fluid through 0.22-μm filters (Millipore). The CTXΦ ΔVC1464 repressor was deleted in order to eliminate phage immunity (28). ΔVC1464 was grown planktonically or in plastic tube-biofilms, as described under "culture conditions." Harvested cells were normalized to an OD_{560} of 1.0 and mixed in a 1:100 ratio with CTX-Km Φ cells for 30 min at 30 °C. After 30 min, cells were plated on LB plates and LB plates containing Km (50 μg/mL) plates, and the percentage of transduced cells was calculated using Km-resistant colonies divided by the total cfu. Three biological replicates were analyzed. Two-tailed unpaired Student's *t*-tests were used for statistical analyses for all experiments using the Prism 8 software (GraphPad Software, Inc.).

MiPACT-HCR.

Fixation. Mouse intestines (groups of 5 mice) were removed at the indicated time points and immediately fixed in methacarn solution (10% acetic acid, 30% chloroform, and 60% methanol).

Embedding. Samples were incubated in 50-mL conical tubes with 20 mL of B4P1 (4% acrylamide/bis-acrylamide mix [29:1], 1% paraformaldehyde, and 0.25% VA-044 in 1× PBS) overnight at 4 °C with gentle rocking. Intestines were then strung through a rubber tube (~15 cm long and 0.5-cm inner diameter), which was subsequently placed in a glass screw-cap tube. The glass tube was filled with fresh B4P1, left open for 5 min in an anaerobic chamber, and then sealed and removed from the chamber. Sealed tubes were then incubated at 37 °C in a water bath for 3 h for acrylamide polymerization. After polymerization, the rubber tube (with embedded intestines inside) was removed from the glass tube, and the acrylamide-embedded intestine was then removed from the rubber tube. The large intestine was separated from the small intestine, and small intestines were cut into four equal-length segments. All embedded samples were stored in 1× PBS with 0.05% sodium azide at 4 °C until further processing.

Clearing. Samples were incubated in a clearing chamber filled with 6–8% sodium dodecyl sulfate (SDS) in 1× PBS, pH 8.0 at 37 °C for 24 h with stirring (43). Samples were removed, washed 3 times with 1 mL 1× PBS (each wash for 20 min on a rocking platform), and then incubated in 1 mL of 1 mg/mL proteinase K in 10 mM Tris·HCl (pH 7.6), shaking at 37 °C for 3 h. Samples were incubated again in the clearing chamber for 24 h and washed in 1× PBS.

Initiator probe HCR hybridization. Approximately 1-mm-long intestine samples were cut from the intestine segments ($n \geq 2$). HCR on cleared samples was performed as described in DePas 2016 with some modifications (13). Briefly, samples were incubated in 1 mL of hybridization buffer (25% formamide, 2X sodium chloride-sodium citrate [SSC], 10% dextran sulfate) with 1 μM of an single-stranded DNA (ssDNA) primer (for blocking) and 30 nM rRNA initiator probes or 10 nM mRNA initiator probes on a 46 °C shaking (250 rpm) heat block for 48 h. To identify *V. cholerae*, a specific rRNA probe [Vchomim1276, 5′-ACT TTG TGA GAT TCG CTC CAC CTC G -3′ (44)] was conjugated to the B4 HCR initiator sequence using HCR 2.0 (17). For *tcpA*-mRNA identification, 10 probes complementary to the *tcpA*-mRNA sequence were conjugated to the B1 HCR initiator sequence using HCR 3.0 (16). HCR 3.0 probes and hairpins were ordered from Molecular Technologies. Samples were washed in 50 mL of hybridization wash buffer (84 mM NaCl, 20 mM Tris·HCl pH 7.6, 5 mM ethylenediaminetetraacetic acid (EDTA) pH 7.2, 0.01% SDS) in a 52 °C water bath for 6 h.

HCR amplification. B1 initiator probes were coupled to Alexafluor647-conjugated hairpins, and B4 initiator probes were coupled to Alexafluor488-conjugated hairpins. Hairpin pairs were prepared individually by heating to 95 °C for 1.5 min in a thermocycler in PCR tubes. They were then cooled at room temperature for 30 min. Each hairpin in a pair was added to 120 nM in 120 μL amplification buffer (2× SSC, 10% dextran sulfate). Samples were incubated with gentle shaking at room temperature for 24 h. Samples were then washed in 50 mL of amplification buffer (337.5 mM NaCl, 20 mM Tris·HCl pH 7.6, 5 mM EDTA pH 7.2, 0.01% SDS) in a 48 °C water bath for 3 h.

Staining and RIMS. Samples were incubated in 1 mL of 1× PBS with 5 μg/mL DAPI (from a dimethyl sulfoxide (DMSO)-suspended stock) for 24 h at room temperature with gentle rocking. After washing 2× with 1 mL of 1× PBS, samples were incubated in 400 μL of RIMS (refractive index matching solution) + 1 μg/mL DAPI until imaging.

Cultured cell controls. For *tcpA* HCR specificity controls (*SI Appendix*, Fig. S4), pTAC::*toxT* and pTAC::*toxT* Δ*tcpA* strains were grown at 30 °C in the presence or absence of 1 mM IPTG until they reached an OD_{600} of ~1.0. Cells were then spun down, resuspended in 1× PBS by pipetting, fixed, and embedded. Wild-type *V. cholerae* or a Δ*tcpA* strain were also grown as biofilms in vitro. After 48 h of growth, biofilm-grown cells were prepared by scraping into 1× PBS and resuspended by pipetting, fixed with 4% paraformaldehyde, and cells were diluted to 0.36 OD_{600} and embedded in 1 mL of B4P1. HCR with Vchomim1276 and the *tcpA*-specific probes were performed as described for the intestine samples.

Image Analysis. To capture a comprehensive view of intestinal colonization, we used a 10X air immersion, numerical aperture 0.45 objective to image the entire circumference of the intestine to 100 μm in depth. To detect bacterial biomass in the intestine and measure its abundance, images were analyzed using BiofilmQ, a software tool we developed for quantifying spatially resolved biofilm properties, which is available at https://drescherlab.org/data/BiofilmQ. This 3D image analysis encompassed the following key steps: After applying a convolution filter to decrease image noise, biomass was identified by thresholding the images in the 488-nm channel. The lumen was detected analogously from fluorescence images in the 405-nm channel. To quantify bacterial location and abundance relative to the crypts and lumen in different sections, a Matlab script was developed, which identified crypts based on the radial intensity profile of the fluorescence image proceeding from the center of the lumen or, in cases where the positions of the crypts were unclear, based on manual user input. At least two intestinal segments were analyzed from each mouse ($n = 5$).

For the analysis of *tcpA*-mRNA abundance and spatial location in the intestine, bacterial cells and their position relative to the lumen and crypts were obtained in the 488-nm channel by the same analysis as described above and for each cell. The integrated as well as mean intensity of the 647-nm channel, which measures the *tcpA*-reporter activity, was calculated using BiofilmQ. At least two intestinal segments were analyzed from each mouse ($n = 5$).

Analysis of *tcp* Production. Cells were grown in LB with or without the addition of 1 mM IPTG and imaged using an AxioImager light microscope with a 20X air immersion, numerical aperture 0.3 objective ($n = 2$). For Western blot analysis, cells were either grown as planktonic or biofilms. Protein pellets from whole cells were suspended in 2% SDS, and protein concentrations were estimated using a Pierce BCA protein assay kit (Thermo Scientific). Equal amounts of total protein (15 μg) were loaded onto an SDS 13% polyacrylamide gel electrophoresis (SDS/PAGE). Western blot analyses were performed as described using anti-TcpA polyclonal antiserum ($n = 2$).

Data Availability. RNA-seq data are available through NCBI GEO with series number GSE135887.

ACKNOWLEDGMENTS. We thank Benjamin Abrams, University of California, Santa Cruz (UCSC) Life Sciences Microscopy Center, for technical support during confocal imaging, which is supported by grant S10 OD023528 (to F.H.Y.) from the National Institutes of Health. We thank Ron Taylor and Karen Skorupski for the TcpA antibody. We thank Adam Alpine for his assistance with Fig. 2 *A* and *B*. We thank Molecular Technologies (Caltech) for assistance with HCR probe design. We would also like to acknowledge the members of the F.H.Y. laboratory and Karla J. F. Satchell for their useful input and contributions. This work was supported by NIH grants RO1 AI102584, RO1 AI114261, and RO1 AI055987 (to F.H.Y.); NIH grants 5R01HL117328-03 and 1R01AI127850-01A1 (to D.K.N.); and the DEPAS17F0 fellowship from the Cystic Fibrosis Foundation (to W.H.D.), as well as the European Research Council StG-716734, the Human Frontier Science Program CDA00084/2015-C, and the Deutsche Forschungsgemeinschaft SFB987 (to K.D.). A.L.G.-H. was supported by the University of California Institute for Mexico and the United States (UC MEXUS) and El Consejo Nacional de Ciencia y Tecnología (CONACYT) Postdoctoral Research fellowship.

1. J. D. Clemens, G. B. Nair, T. Ahmed, F. Qadri, J. Holmgren, Cholera. *Lancet* **390**, 1539–1549 (2017).
2. WHO, *Cholera*, (WHO, Geneva, Switzerland, 2017).
3. R. Tamayo, B. Patimalla, A. Camilli, Growth in a biofilm induces a hyperinfectious phenotype in *Vibrio cholerae*. *Infect. Immun.* **78**, 3560–3569 (2010).
4. J. K. Teschler *et al*., Living in the matrix: Assembly and control of *Vibrio cholerae* biofilms. *Nat. Rev. Microbiol.* **13**, 255–268 (2015).
5. J. G. Conner, J. K. Teschler, C. J. Jones, F. H. Yildiz, "Staying alive: *Vibrio cholerae*'s cycle of environmental survival, transmission, and dissemination" in *Virulence Mechanisms of Bacterial Pathogens*, (American Society of Microbiology, ed. 2, 2016), pp. 593–633.
6. C. Matz *et al*., Biofilm formation and phenotypic variation enhance predation-driven persistence of *Vibrio cholerae*. *Proc. Natl. Acad. Sci. U.S.A.* **102**, 16819–16824 (2005).
7. S. Beyhan, F. H. Yildiz, Smooth to rugose phase variation in *Vibrio cholerae* can be mediated by a single nucleotide change that targets c-di-GMP signalling pathway. *Mol. Microbiol.* **63**, 995–1007 (2007).
8. R. R. Colwell *et al*., Reduction of cholera in Bangladeshi villages by simple filtration. *Proc. Natl. Acad. Sci. U.S.A.* **100**, 1051–1055 (2003).
9. S. M. Faruque *et al*., Transmissibility of cholera: In vivo-formed biofilms and their relationship to infectivity and persistence in the environment. *Proc. Natl. Acad. Sci. U.S.A.* **103**, 6350–6355 (2006).
10. A. T. Nielsen *et al*., A bistable switch and anatomical site control *Vibrio cholerae* virulence gene expression in the intestine. *PLoS Pathog.* **6**, e1001102 (2010).
11. A. T. Nielsen *et al*., RpoS controls the *Vibrio cholerae* mucosal escape response. *PLoS Pathog.* **2**, e109 (2006).
12. A. Stacy, L. McNally, S. E. Darch, S. P. Brown, M. Whiteley, The biogeography of polymicrobial infection. *Nat. Rev. Microbiol.* **14**, 93–105 (2016).
13. W. H. DePas *et al*., Exposing the three-dimensional biogeography and metabolic states of pathogens in cystic fibrosis sputum via hydrogel embedding, clearing, and rRNA labeling. *MBio* **7**, e00796-16 (2016).
14. B. Yang *et al*., Single-cell phenotyping within transparent intact tissue through whole-body clearing. *Cell* **158**, 945–958 (2014).
15. C. Fung *et al*., High-resolution mapping reveals that microniches in the gastric glands control *Helicobacter pylori* colonization of the stomach. *PLoS Biol.* **17**, e3000231 (2019).
16. H. M. T. Choi *et al*., Third-generation *in situ* hybridization chain reaction: Multiplexed, quantitative, sensitive, versatile, robust. *Development* **145**, dev165753 (2018).
17. H. M. T. Choi, V. A. Beck, N. A. Pierce, Next-generation in situ hybridization chain reaction: Higher gain, lower cost, greater durability. *ACS Nano* **8**, 4284–4294 (2014).
18. K. Nikolakakis, E. Lehnert, M. J. McFall-Ngai, E. G. Ruby, Use of hybridization chain reaction-Fluorescent in situ hybridization to track gene expression by both partners during initiation of symbiosis. *Appl. Environ. Microbiol.* **81**, 4728–4735 (2015).
19. R. Hartmann *et al*., BiofilmQ, a software tool for quantitative image analysis of microbial biofilm communities. bioRxiv:735423 (15 August 2019).
20. Y. A. Millet *et al*., Insights into *Vibrio cholerae* intestinal colonization from monitoring fluorescently labeled bacteria. *PLoS Pathog.* **10**, e1004405 (2014).
21. S. Ménard *et al*., Developmental switch of intestinal antimicrobial peptide expression. *J. Exp. Med.* **205**, 183–193 (2008).
22. A. L. Gallego-Hernandez, J. H. Park, J. K. Teschler, S. Beyhan, F. H. Yildiz, Vibrio cholerae biofilm and planktonic growth RNAseq analysis. National Center for Biotechnology Information Gene Expression Omnibus. https://www.ncbi.nlm.nih.gov/geo/query/acc.cgi?acc=GSE135887. Deposited 15 August 2019.
23. R. K. Taylor, V. L. Miller, D. B. Furlong, J. J. Mekalanos, Use of *phoA* gene fusions to identify a pilus colonization factor coordinately regulated with cholera toxin. *Proc. Natl. Acad. Sci. U.S.A.* **84**, 2833–2837 (1987).
24. R. A. Finkelstein, J. J. LoSpalluto, Pathogenesis of experimental cholera. Preparation and isolation of choleragen and choleragenoid. *J. Exp. Med.* **130**, 185–202 (1969).
25. N. K. Dutta, M. V. Panse, D. R. Kulkarni, Role of cholera a toxin in experimental cholera. *J. Bacteriol.* **78**, 594–595 (1959).
26. M. K. Waldor, J. J. Mekalanos, Lysogenic conversion by a filamentous phage encoding cholera toxin. *Science* **272**, 1910–1914 (1996).
27. H. H. Kimsey, M. K. Waldor, CTXphi immunity: Application in the development of cholera vaccines. *Proc. Natl. Acad. Sci. U.S.A.* **95**, 7035–7039 (1998).
28. E. J. Kim *et al*., Replication of *Vibrio cholerae* classical CTX phage. *Proc. Natl. Acad. Sci. U.S.A.* **114**, 2343–2348 (2017).
29. T. Bjarnsholt, The role of bacterial biofilms in chronic infections. *APMIS Suppl.* **121**, 1–51 (2013).
30. S. Furukawa, S. L. Kuchma, G. A. O'Toole, Keeping their options open: Acute versus persistent infections. *J. Bacteriol.* **188**, 1211–1217 (2006).
31. B. Mudrak, R. Tamayo, The *Vibrio cholerae* Pst2 phosphate transport system is upregulated in biofilms and contributes to biofilm-induced hyperinfectivity. *Infect. Immun.* **80**, 1794–1802 (2012).
32. F. H. Yildiz, N. A. Dolganov, G. K. Schoolnik, VpsR, a member of the response regulators of the two-component regulatory systems, is required for expression of *vps* biosynthesis genes and EPS(ETr)-associated phenotypes in *Vibrio cholerae* O1 El Tor. *J. Bacteriol.* **183**, 1716–1726 (2001).
33. F. H. Yildiz, X. S. Liu, A. Heydorn, G. K. Schoolnik, Molecular analysis of rugosity in a *Vibrio cholerae* O1 El Tor phase variant. *Mol. Microbiol.* **53**, 497–515 (2004).
34. S. Beyhan, K. Bilecen, S. R. Salama, C. Casper-Lindley, F. H. Yildiz, Regulation of rugosity and biofilm formation in *Vibrio cholerae*: Comparison of VpsT and VpsR regulons and epistasis analysis of *vpsT*, *vpsR*, and *hapR*. *J. Bacteriol.* **189**, 388–402 (2007).
35. J. Zhu, J. J. Mekalanos, Quorum sensing-dependent biofilms enhance colonization in *Vibrio cholerae*. *Dev. Cell* **5**, 647–656 (2003).
36. W. Lin, G. Kovacikova, K. Skorupski, The quorum sensing regulator HapR downregulates the expression of the virulence gene transcription factor AphA in *Vibrio cholerae* by antagonizing Lrp- and VpsR-mediated activation. *Mol. Microbiol.* **64**, 953–967 (2007).
37. National Academies Press, *Guide for the Care and Use of Laboratory Animals*, (National Academies Press, Washington, D.C., 2011).
38. B. Lim, S. Beyhan, J. Meir, F. H. Yildiz, Cyclic-diGMP signal transduction systems in *Vibrio cholerae*: Modulation of rugosity and biofilm formation. *Mol. Microbiol.* **60**, 331–348 (2006).
39. A. T. Cheng, K. M. Ottemann, F. H. Yildiz, *Vibrio cholerae* response regulator VxrB controls colonization and regulates the Type VI Secretion System. *PLoS Pathog.* **11**, e1004933 (2015).
40. V. Baselski, R. Briggs, C. Parker, Intestinal fluid accumulation induced by oral challenge with *Vibrio cholerae* or cholera toxin in infant mice. *Infect. Immun.* **15**, 704–712 (1977).
41. R. Schmieder, Y. W. Lim, R. Edwards, Identification and removal of ribosomal RNA sequences from metatranscriptomes. *Bioinformatics* **28**, 433–435 (2012).
42. M. D. Robinson, D. J. McCarthy, G. K. Smyth, edgeR: A Bioconductor package for differential expression analysis of digital gene expression data. *Bioinformatics* **26**, 139–140 (2010).
43. A. Greenbaum *et al*., Bone CLARITY: Clearing, imaging, and computational analysis of osteoprogenitors within intact bone marrow. *Sci. Transl. Med.* **9**, eaah6518 (2017).
44. S. Schauer, R. Sommer, A. H. Farnleitner, A. K. T. Kirschner, Rapid and sensitive quantification of *Vibrio cholerae* and *Vibrio mimicus* cells in water samples by use of catalyzed reporter deposition fluorescence in situ hybridization combined with solid-phase cytometry. *Appl. Environ. Microbiol.* **78**, 7369–7375 (2012).